NASA CONTRACTOR REPORT

NASA CR-1507

ANALYSIS OF LARGE BENDING DEFORMATIONS OF A FILAMENTARY TUBULAR SHELL TYPICAL FOR PRESSURE CONSTRAINT COMPONENTS OF SPACE SUITS

by Odus R. Burggraf

Prepared by
ASTRO RESEARCH CORPORATION
Santa Barbara, Calif.
for

NATIONAL AERONAUTICS AND SPACE ADMINISTRATION • WASHINGTON, D. C. • JANUARY 1970

NASA CR-1507

ANALYSIS OF LARGE BENDING DEFORMATIONS OF A FILAMENTARY TUBULAR SHELL TYPICAL FOR PRESSURE CONSTRAINT COMPONENTS OF SPACE SUITS

By Odus R. Burggraf

Issued by Originator as Report No. ARC-R-331

Prepared under Contract No. NAS 7-728 by
ASTRO RESEARCH CORPORATION
Santa Barbara, Calif.

for

NATIONAL AERONAUTICS AND SPACE ADMINISTRATION

For sale by the Clearinghouse for Federal Scientific and Technical Information
Springfield, Virginia 22151 – Price $3.00

ABSTRACT

A theory is formulated for the bending deformation of a cylindrical, pressurized fiber shell, including the effects of fiber slippage. This type of structure is representative for pressure constraint components of space suits.

Special consideration is given to the filament-wound and linked-fiber tube in the postslip phase of bending, although any type of knots or fixed fiber nodes are permitted in the preslip phase. Inextensible fibers are assumed throughout. Analytical formulas are derived for the bending characteristics, including bending stiffness, in the range of small deformations, and numerical results are obtained for large deformations. The idealized frictionless-fiber tube is shown to be unstable in bending. For the friction-stabilized tube constructed from pairs of left-running and right-running fibers, the effect of the variable-mesh parallelogram in the preslip phase is to produce a wide linear range followed by a relatively flat moment characteristic for large bending angles. The effect of fiber slippage is to produce a rapid reduction of the bending moment required for deformation with ultimate destabilization as the bending angle increases.

CONTENTS

INTRODUCTION

Deformable fibermesh structures are required in the pressure constraints of "soft" space suit components. This report presents the analysis of a special type of pressurized fibermesh structure. The undeformed configuration is assumed to be a circular cylinder; the deformation caused by bending moment results in a deformed state corresponding to a segment of a torus. Since large deformations are considered, the analysis allows for noncircular cross section. To permit the analytical simplification of axial symmetry, end constraints are assumed that allow plane sections, initially perpendicular to the axis of the cylinder, to remain plane under bending deformation. However, the section may rotate through large angles. This assumption is not expected to be valid near the ends for realistic end conditions, but should be a good approximation over the main part of the structure.

The problem is formulated by analyzing a family of toroids, segments of which represent a cylindrical fiber tube deformed by bending moments. The analysis is based on the fiber-equilibrium model used previously (Ref. 1). Basically, this model corresponds to a pair of overlying monotropic membranes in which the stress resultants come about solely from the tension-loaded inextensible fibers. In Reference 1 this model was applied to the case of frictionless noninteracting fibers; in the present case, we include the effect of interfiber friction arising from the tendency of the fibers to slide over one another during bending. All the geometric properties of the structure are made available as a result of this analysis. The various members of the family of toroids considered then represent the different stages of deformation of some original cylinder. The particular sequence of toroidal segments corresponding to a given initial cylindrical slip-net are identified by use of the following constraints:

1) Filament length - the length of fiber in one complete loop wound about the cylinder remains invariant under deformation.

2) Number of fibers - the number of fibers crossing a generator of the cylinder in a distance corresponding to one fiber loop is invariant under deformation.

3) <u>Closed-loop fiber curves</u> - the curvature of the cross-sectional curve of the toroids must be finite everywhere, since the filamentary shell carries the entire structural load, consisting of end-moment and internal pressure.

4) <u>Pressure-volume relation</u> - the pressurizing gas (or liquid) is subject to a thermodynamic equation of state. Normally, the adiabatic relation (pV^{γ} = constant) is appropriate (p = pressure, V = volume). For a very slow process, the isothermal law (pV = constant) is the correct equilibrium condition. Alternatively, the tube may be connected to a large reservoir, in which case the isobaric relation (p = constant) is applicable.

Applying these constraints to the solution resulting from the fiber-equilibrium analysis, a one-parameter family of toroids is obtained, corresponding to the various deformed states, under bending, of the original cylindrical fiber shell.

In the following analysis, two distinct states of bending are distinguished: (a) preslip deformation and (b) postslip deformation. The distinction is that the preslip state of bending is characterized by such large friction (or small bending moment) that the overlapping fibers cannot slide. The elemental lengths of the two-fiber mesh pattern then remain invariant, the deformation arising through "shear" of the elemental fiber pattern as a kinematic linkage. On the other hand, a three-fiber mesh constitutes a structure, and deformation results only from extension of the fibers. The postslip state of bending is characterized by the fibers sliding over each other with constant sliding friction; the elemental lengths of the fiber pattern are no longer invariant.* By choosing distinct values of starting friction and sliding friction, a hysteresis pattern of the deformation history can be obtained.

One application of the theory developed here is to the "slip-net" structure, invented by A. C. Kyser. The slip-net is a filamentary pressure vessel constructed in such a way that the load-carrying fibers are free to slip over one another with

*This model has the obvious analogy of perfectly plastic flow (Prager and Hodge, Ref. 2).

small friction, thus permitting large bending deformations with very low stiffness and restoring moment. Discussion and some applications of these structures are given in Reference 3.

LIST OF SYMBOLS

a	radius of three-fiber tube
A_j	coefficient of the j^{th}-order term in series development
b	tube length
B	constant membrane force of three-fiber tube
c	$= \sin\beta_1$
d	tube diameter
E	strain energy
f	friction coefficient
F'	friction force per unit fiber length
F_N	interfiber node force
$F(k)$	complete elliptic integral of the first kind
$I_1, I_2, I^{(j)}$	integrals
j	index in series development
k	modulus of elliptic integrals
K	pressure parameter, see Equation (9)
ℓ	fiber length
L	$= \frac{\ell}{r_1}$, nondimensional fiber length
m	total number of fibers crossing the meridian
m'	number of fibers crossing unit length of meridian
M	bending moment

n	total number of fibers
n'	fiber number of single family per unit length
p	pressure
r	radial coordinate
R	$= \frac{r}{r_1}$, nondimensional radial coordinate
T	fiber tension
u	amplitude of elliptic integral
V	volume of tube
W	pressure-volume work
x	$= R^2$
x_2, x_3	roots of cubic expression, see Equation (12)
z	axial coordinate
Z	$= \frac{z}{r_1}$, nondimensional axial coordinate
α	angle between meridian and z-axis
α^2	parameter of elliptic integral of the third kind
β	angle between fiber and meridian
$\overline{\beta}$	$= \frac{\pi}{2} - \beta$
γ	adiabatic exponent
ϵ	strain
$\delta\theta$	angle between rays on the tangent cone passing through adjacent fiber nodes

φ	central angle of bent tube
ψ	argument of trigonometric functions in elliptic integrals

Subscripts:

$\ldots_0$	undeformed state
$\ldots_1$	values at maximum radius in bent state
$\ldots_2$	values at minimum radius in bent state
$\ldots_C$	circumferential
$\ldots_L$	left wound
$\ldots_R$	right wound

EQUILIBRIUM CONDITIONS FOR FIBER NODES

The main part of our discussion will be restricted to a two-fiber model; that is, each fiber node represents the intersection of only two fibers forming a symmetric pattern of left-running and right-running filaments. The case of a three-fiber shell is treated in a later section. We consider an axisymmetric structure loaded only by internal pressure and interfiber forces (see Figures 1 and 2.)

Consider a control surface about a representative fiber node. This surface cuts the fibers halfway between adjacent nodes. The fibers lie at an angle, β, relative to the meridian curves on the shell of revolution as shown in Figure 2. Then equilibrium of forces on the control surface in the direction parallel to the tangent to the meridian curve at the fiber node is expressed by the equation

$$(T + \delta T) \cos\left(\beta + \delta\beta - \frac{\delta\theta}{2}\right) = T \cos\left(\beta + \frac{\delta\theta}{2}\right)$$

where T is the fiber tension and $\delta\theta$ the angle between rays, on the tangent cone, passing through adjacent nodes. For a dense fiber pattern, δT, $\delta\beta$, and $\delta\theta$ are all small and will be regarded as differentials. Then the above equilibrium equation becomes

$$\delta T \cos\beta - T\left(\delta\beta - \frac{\delta\theta}{2}\right) \sin\beta = - T\left(\frac{\delta\theta}{2}\right) \sin\beta$$

or

$$\delta\beta = \frac{\delta T}{T} \cot\beta + \delta\theta \tag{1}$$

Now denote by $\delta\ell$ the length of fiber between nodes. Also let r be the radius to the shell surface at the node measured from the axis of revolution of the deformed shell (torus). Then δr represents the incremental radius between nodes, and we have

$$\delta\theta = -\frac{\delta r}{r}\tan\beta \qquad (2)$$

With this result, Equation 1 becomes

$$\delta\beta = \frac{\delta T}{T}\cot\beta - \frac{\delta r}{r}\tan\beta$$

This equation can be expressed in the simpler form

$$\frac{d}{dr}(Tr\sin\beta) = r\frac{dT}{dr}\csc\beta \qquad (3)$$

Clearly the isotensoid fiber shell (T = constant) corresponds to the geodesic condition, $r\sin\beta$ = constant, derived previously (Refs. 1 and 3).

Now denote α to be the angle between the axis of revolution and the tangent to the meridian curve, as shown in Figure 1. The fiber force parallel to the z-axis at radius, r, is

$$n\,T\cos\beta\cos\alpha$$

where n is the total number of fibers, both right-running and left-running, crossing the circumference of the toroidal shell. Then considering an annular region of the shell of radial depth, dr, the equilibrium condition parallel to the z-axis is

$$\frac{d}{dr}\left(T\cos\beta\cos\alpha\right) = \frac{2\pi}{n}pr \qquad (4)$$

where p is the pressure difference across the shell. Equations 3 and 4 constitute two equations for the three unknowns T, α, and β. The third equation is obtained by considering the geometric constraint imposed by a non-sliding fiber mesh.

The initial undeformed mesh is composed of fibers in two contrawound families. The elemental mesh configuration, then, is a parallelogram, and the deformed elemental mesh is a parallelogram having the same fiber lengths but varying diagonals. The circumferential diagonal has length $4\pi\, r/n$, and also $2\, \delta\ell \sin\beta$, by definition of β. Here $\delta\ell$ is the distance between adjacent fibers, measured along a fiber of opposite family. Equating these two expressions yields

$$r \csc\beta = \frac{n}{2\pi}\, \delta\ell \tag{5}$$

Since $\delta\ell$ is constant over the surface of the cylindrical slipnet, the geometrical constraint in the preslip deformed state is just

$$r \csc\beta = \frac{r_1}{c} = \text{constant} \tag{6}$$

where r_1 is the maximum shell radius and $c = \sin\beta_1$ is the fiber angle evaluated at r_1. Equation 6 replaces the geodesic condition, $r \sin\beta = \text{constant}$, that holds for the isotensoid structure.

Utilizing Equation 6 in the form

$$\sin\beta = cR \tag{7}$$

where R is non-dimensional radius (r/r_1), we can now integrate Equation 3 immediately to obtain

$$\left(\frac{T}{T_1}\right) = \frac{1 - c^2}{1 - c^2 R^2} \tag{8}$$

The angle, α, is now determined by integrating Equation 4. Denoting the pressure parameter, K, as

$$K = \frac{2\pi\, p r_1^2}{n\, T_1} \tag{9}$$

and requiring $\alpha = 0$ for $r = r_1$, we find

$$\cos\alpha = \frac{\sqrt{1 - c^2 R^2}}{1 - c^2} \left[\sqrt{1 - c^2} - \frac{1}{2} K \left(1 - R^2\right)\right] \tag{10}$$

from which

$$\sin\alpha = \frac{\sqrt{1 - R^2}}{1 - c^2} \left\{ \left[K \sqrt{1 - c^2} - \frac{K^2}{4}\left(1 - R^2\right)\right] \left(1 - c^2 R^2\right) - c^2 \left(1 - c^2\right)\right\}^{\frac{1}{2}}$$

In factored form, with $x = R^2$,

$$\sin\alpha = \frac{Kc}{2\left(1 - c^2\right)} \sqrt{\left(x_3 - x\right)\left(1 - x\right)\left(x - x_2\right)} \tag{11}$$

where

$$x_{2,\,3} = \frac{1 + c^2}{2c^2} - \frac{2}{K} \sqrt{1 - c^2} \mp \frac{1 - c^2}{2c^2} \sqrt{1 + \frac{8c^2}{K\sqrt{1 - c^2}}} \tag{12}$$

Clearly both roots x_2 and x_3 are real. The root, x_2 , is chosen to correspond to $\alpha = \pi$ (minimum radius of torus). The following conditions on the roots can be proven:

TYPE A: $\quad x_2 < x < 1 < x_3 < \frac{1}{c^2}$ if $K > \frac{c^2}{\sqrt{1 - c^2}}$ (13)

$$\text{TYPE B:} \qquad x_2 < x < x_3 < 1 \quad \text{for} \quad 0 < K < \frac{c^2}{\sqrt{1 - c^2}} \tag{14}$$

This order of x_2 , x , x_3 follows from Equation 11 so that $\sin\alpha$ is real. Clearly in Type B x_3 is the maximum radius, so that by rescaling r_1 , the solutions of Type B can be scaled into those of Type A. Henceforth we consider only Type A.*

A formula for values of K for given $x_2 = R^2_{min}$ is obtained from Equation 10 by setting $\cos\alpha = -1$:

$$K = \frac{2\sqrt{1 - c^2}}{1 - R^2_{min}} \left[1 + \sqrt{\frac{1 - c^2}{1 - c^2 R^2_{min}}}\right] \tag{15}$$

Consequently, for closed-loop toroids $K \geq 2\sqrt{1 - c^2}\left(1 + \sqrt{1 - c^2}\right)$. Also, note that real values of K are obtained for any R_{min} in the range $0 \leq R_{min} \leq 1$. This is in contrast to the case of toroidal isotensoids, for which $c \leq R_{min} \leq 1$.

Most of the formulas above were derived subject to the mesh constraint given by Equation 6. Since this constraint holds only if the fibers do not slip, the range of applicability of these formulas is determined by the condition of incipient slip. This condition, in turn, depends on the configuration of the fibers at the node. We shall consider two types of fiber mesh: the mesh constructed by winding fibers continuously along the tube and the mesh constructed by linking fibers such that any continuous fiber alternates back and forth as it passes around the tube. These mesh types may be regarded as degenerate cases of more general knotted nodes.

---

*A third type of ordering exists for which $x_2 < x_3 < 1 < x$ with $K < c^2/1 - c^2$. However, closed-loop toroids are not possible under this condition.

First consider the filament-wound tube. The forces acting in the tangent plane on a single continuous fiber (see Fig. 3) are the fiber tension and the frictional interaction force. Let F' denote the frictional force per unit length of fiber. Symmetry requires that F' act in the direction perpendicular to the meridian plane. Consequently

$$F'\delta\ell = (T + \delta T)\ \sin\left(\beta + \delta\beta - \frac{\delta\theta}{2}\right) - T\ \sin\left(\beta + \frac{\delta\theta}{2}\right)$$

Again treating the incremental quantities as differentials, and making use of Equation 2 and the geometric relationship

$$\delta r = -\ \delta\ell\ \cos\beta\ \sin\alpha$$

we find

$$rF' = -\left[\frac{d}{dr}\left(Tr\ \sin\beta\right)\right]\cos\beta\ \sin\alpha \tag{16}$$

Utilizing Equation 3

$$\frac{dT}{dr} = -\ F'\ \tan\beta\ \csc\alpha \tag{17}$$

The frictional force, F' , is assumed to be proportional to the normal force supported by the fiber, due to pressure loading. For a fiber of length, $\delta\ell$, the total fiber length for a complete annulus is $n\delta\ell$. The surface area of the annulus is $2\pi r\delta\ell\ \cos\beta$. Hence the normal force supported per unit length of each fiber is

$$\frac{2\pi pr\ \cos\beta}{n}$$

Thus we find the limiting frictional interaction force is

$$F'_{lim} = \pm\ f\ \frac{2\pi pr\ \cos\beta}{n} \tag{18}$$

where f is the friction coefficient. Recalling the definition of K by Equation 9, the no-slip condition then results from Equations 17 and 18 as

$$\left|\frac{d}{dR}\left(\frac{T}{T_1}\right)\right| \leq fKR \sin\beta \csc\alpha \tag{19}$$

Taken as an equality, Equation 19 serves as an equilibrium equation for the postslip analysis, replacing the no-slip mesh constraint, Equation 6. If the mesh has not slipped locally, the derivative of the tension can be evaluated from Equation 8. In this way, Equations 17 and 18 yield

$$\sin\alpha \leq \frac{fKR}{2c(1 - c^2)} \cos^4\beta \tag{20}$$

A value of one for this ratio is the condition for incipient slip.

Now consider the linked-fiber tube (see Fig. 4). The inter-fiber node force, F_N, acts in the direction perpendicular to the meridian plane, by symmetry, and exists in this case even for frictionless fibers. It has the value

$$F_N = 2T \sin\beta \tag{21}$$

The incremental tension, δT, across the node is sustained by the frictional drag between the linked fibers, proportional to F_N. Hence for incipient slip

$$\delta T = 2fT \sin\beta \tag{22}$$

where f is the friction coefficient for the fibers. Again we conclude that the frictionless fiber structure is an isotensoid, and that the fiber geometry and shape of meridian curve are identical for the frictionless filament-wound shell and the frictionless linked-fiber shell. However, in the event of fiber slippage, the frictional effects are different for these two types of fiber shells. Equation 22 gives the increment of tension across a single node. Let m' be the number of fibers of both families crossing a unit length of meridian curve. Then we find

$$\left|\frac{dT}{dr}\right| \leq 2f\, m'\, T \sin\beta \csc\alpha \tag{23}$$

where the equality is taken as the no-slip limit. In addition, continuity of fibers requires

$$m' = \frac{n}{2\pi r} \tan\beta \tag{24}$$

Again if the mesh has not slipped locally, combining Equations 7, 23, and 24, and using Equation 8 to evaluate the derivation yields the condition

$$\sin\alpha \leq \frac{fn}{2\pi} \cos\beta \tag{25}$$

Taken as an equality, Equation 25 is the condition for incipient slip of the linked fiber tube. It is interesting that when the friction limit is exceeded the fiber count, n , appears as an independent parameter for the linked mesh, but not for the filament-wound tube.

GEOMETRIC PROPERTIES OF THE PRESLIP BENDING STATE

The simplest property of the preslip state of deformation is a relation between filament length and central angle (i.e. angle through which the fiber tube is bent). By geometry, we have the relation for differential length along a fiber

$$d\ell \sin\beta = r d\varphi$$

Utilizing Equation 6, we find

$$\varphi = c \frac{\ell}{r_1} \tag{26}$$

This equation restates the assumption that plane sections remain plane under bending deformation of the original cylinder.

To apply the four constraints mentioned in the preceding section, we need three more geometrical properties: filament length, shape of meridian curve, and volume. Unfortunately, these properties are all determinable as hyperelliptic integrals. They may be expressed as integrals of Jacobian elliptic functions depending on only two parameters, and so are easy to evaluate numerically.* These integral formulas are derived here.

Denote the non-dimensional fiber length as

$$L = \frac{\ell}{r_1}$$

Then from the fiber geometry

$$\frac{dL}{dR} = -\sec\beta \csc\alpha = \frac{-\csc\alpha}{\sqrt{1 - c^2 R^2}}$$

*See Reference 4 (Milne-Thomson) for tabulations of Jacobian elliptic functions.

From Equation 11 we find for the length of a half-loop ($x_2 < x < 1$)

$$L_2 = \frac{1 - c^2}{Kc^2} \int_{x_2}^{1} \frac{dx}{\sqrt{x\left(\frac{1}{c^2} - x\right)\left(x_3 - x\right)\left(1 - x\right)\left(x - x_2\right)}} \tag{27}$$

Changing variables to introduce the elliptic functions, we find

$$L_2 = \frac{2\sqrt{1 - c^2}}{Kc\sqrt{x_2\left(x_3 - x_2\right)}} \int_0^{F(k)} \left\{\frac{1 - \alpha^2 \operatorname{sn}^2 u}{1 - \left(\frac{\alpha^2}{c^2 x_2}\right)\operatorname{sn}^2 u}\right\}^{1/2} du \tag{28}$$

where $F(k)$ is the complete elliptic integral of first kind, and

$$\left.\begin{aligned} k^2 &= \frac{\left(1 - c^2 x_3\right)\left(1 - x_2\right)}{\left(1 - c^2\right)\left(x_3 - x_2\right)}, \quad \alpha^2 = - c^2\left(\frac{1 - x_2}{1 - c^2}\right) \\ \text{and} \qquad \operatorname{sn}^2 u &= \sin^2\psi = \frac{\left(1 - c^2\right)\left(x - x_2\right)}{\left(1 - x_2\right)\left(1 - c^2 x\right)} \end{aligned}\right\} \tag{29}$$

If c and x_2 are regarded as two independent parameters, all the others in Equations 28 and 29 are determined thereby (with K given by Equation 15); thus L_2 is given by only two free parameters.

In a similar way, the meridian curve can be calculated. Denoting the non-dimensional axial coordinate as

$$Z = \frac{z}{r_1}$$

we have $$\frac{dZ}{dR} = -\cot\alpha$$

Using Equations 10 and 11

$$Z = \pm \frac{1}{K} \int_{x_2}^{x} \frac{\sqrt{\frac{1}{c^2} - x}\left[\sqrt{1 - c^2} - \frac{K}{2}(1 - x)\right]}{\sqrt{x\left(x - x_2\right)\left(1 - x\right)\left(x_3 - x\right)}}\, dx \tag{30}$$

In terms of the variables defined in Equation 29 we find

$$Z = \pm \frac{2}{Kc} \frac{1 - c^2 x_2}{\sqrt{x_2\left(x_3 - x_2\right)}} \left\{ \int_0^u \frac{du}{\left[1 - \alpha^2 \mathrm{sn}^2 u\right]^{\frac{1}{2}} \left[1 - \left(\frac{\alpha^2}{c^2 x_2}\right)\mathrm{sn}^2 u\right]^{\frac{1}{2}}} \right.$$

$$\left. - \frac{K(1 - x_2)}{2\sqrt{(1 - c^2)}} \int_0^u \frac{\mathrm{cn}^2 u \, du}{\left[1 - \alpha^2 \mathrm{sn}^2 u\right]^{\frac{1}{2}} \left[1 - \left(\frac{\alpha^2}{c^2 x_2}\right)\mathrm{sn}^2 u\right]^{\frac{3}{2}}} \right\} \tag{31}$$

The volume is calculated most easily by equating strain energy to pressure-volume work. For a virtual deformation, the pressure-volume work is

$$\delta W = \frac{3}{2}\, \epsilon \, p \, V$$

The total number of fibers over the length of the tube is $n \frac{\varphi}{2\pi}$. Hence the strain energy is

$$\delta E = \frac{n \epsilon \varphi}{4\pi} \int_0^{\ell_1} T \, d\ell$$

Here V is the volume of the tube, and ℓ_1 is the length of a complete fiber turn ($x = 1$ to $x = x_2$ to $x = 1$). Hence the tube volume is given by

$$V = \frac{n\varphi}{6\pi p} \int_0^{\ell_1} T \, d\ell$$

Note that this formula is not limited to the friction-loaded slip-net. Thus for the frictionless isotensoid tube, we have the formula

$$V = \frac{2r_1^3 \varphi L_2}{3K} \tag{32}$$

For the friction-loaded fiber tube, the result is not so simple. By geometry

$$d\ell = - dr \sec\beta \csc\alpha$$

Then from Equations 7, 8, 9, and 11, we have

$$V = \frac{2\varphi r_1^3}{3K^2 c^4} (1 - c^2)^2 \int_{x_2}^{1} \frac{dx}{\left(\frac{1}{c^2} - x\right)^{\frac{3}{2}} \sqrt{x(x - x_2)(1 - x)(x_3 - x)}} \tag{33}$$

Again converting to the Jacobian elliptic-function notation defined in Equation 29, we have

$$V = \frac{4\varphi r_1^3}{3K^2 c} \frac{(1 - c^2)^{\frac{3}{2}}}{(1 - c^2 x_2)\sqrt{x_3(x_3 - x_2)}} \int_0^{F(k)} \frac{(1 - \alpha^2 \, \mathrm{sn}^2 u)^{3/2}}{\left[1 - \left(\frac{\alpha^2}{c^2 x_2}\right) \mathrm{sn}^2 u\right]^{1/2}} du \quad (34)$$

The principal quantity of interest is the applied bending moment that produces the given deformation. This moment is readily formulated from the fiber tension and pressure loading on a given meridian plane, representing the end of our deformed cylinder. However, it is simpler and, as it turns out, numerically more accurate, to apply the energy principle. This method is valid for the preslip condition, but does not account for frictional energy loss during the postslip phase. Equating the work done by the applied moment to the pressure-volume work done on the pressurizing gas*, we have

$$M = - p \frac{dV}{d\varphi} \quad (35)$$

*The fibers have been regarded as inextensible and thus do not absorb any of the energy.

ASYMPTOTIC SOLUTION FOR SMALL DEFORMATION

The formulas derived in the foregoing section constitute a non-linear theory for large deformations. However, no explicit solutions are obtained, but instead a tedious iteration procedure involving numerical, analog, or graphical integration is required for solution. To obtain simple analytical results, we turn to the method of series expansion to generate an explicit solution valid for small deformations. Numerical results for large deformations are presented in a later section.

From the definition of K, the initial undeformed cylinder corresponds to $K \to \infty$ $(r_1 \to \infty)$. Thus, we see that an expansion in powers of $1/K$ is appropriate. We shall later replace K as expansion variable by the more useful bending moment, M. Since all the integrals of the preceding section involve the roots, x_2 and x_3, let us first seek an expansion for these roots. From Equation 12 we see that a radical must be expanded, as follows:

$$\left[1 + \frac{8c^2}{K\sqrt{1 - c^2}}\right]^{\frac{1}{2}} = 1 + \frac{4c^2}{K\sqrt{1 - c^2}} - \frac{8c^4}{K^2(1 - c^2)} + \frac{32c^6}{K^3(1 - c^2)^{\frac{3}{2}}}$$

$$- \frac{160c^8}{K^4(1 - c^2)^2} + \dots$$

Substituting this expansion in Equation 12 yields

$$x_2 = 1 - \frac{4}{K}\sqrt{1 - c^2} + \frac{4c^2}{K^2} - \frac{16c^4}{K^3\sqrt{1 - c^2}} + \frac{80c^6}{K^4(1 - c^2)} + \dots \qquad (36)$$

$$x_3 = \frac{1}{c^2} - \frac{4c^2}{K^2} + \frac{16c^4}{K^3\sqrt{1 - c^2}} - \frac{80c^6}{K^4(1 - c^2)} + \dots \qquad (37)$$

Now, since $x_2 \leq x \leq 1$, from Equation 36 we find

$$1 - x = 0(\frac{1}{K})$$

so that our functions of x can be expanded in powers of $(1 - x)$ as well as powers of $(1/K)$. Thus, for example,

$$x^{-\frac{1}{2}} = [1 - (1 - x)]^{-\frac{1}{2}} = 1 + \frac{1}{2}(1 - x) + \frac{3}{8}(1 - x)^2 + \frac{5}{16}(1 - x)^3$$

$$+ 0\left(\frac{1}{K^4}\right) \tag{38}$$

$$(x_3 - x)^{-\frac{1}{2}} = (x_3 - 1)^{-\frac{1}{2}} \left[1 + \left(\frac{1 - x}{x_3 - 1}\right)\right]^{-\frac{1}{2}} = \frac{1}{\sqrt{x_3 - 1}} \left[1 - \frac{1}{2} \frac{1 - x}{x_3 - 1}\right.$$

$$\left. + \frac{3}{8}\left(\frac{1 - x}{x_3 - 1}\right)^2 - \frac{5}{16} \left(\frac{1 - x}{x_3 - 1}\right)^3\right] + 0\left(\frac{1}{K^4}\right) \tag{39}$$

and the terms in $(x_3 - 1)$ are expandable using the series of Equation 37.

Let us now evaluate $z(x_2)$, which is needed to establish the condition for a closed-loop meridian curve. Equation 30 can be rewritten in terms of two integrals as

$$Z(x_2) = \frac{1}{K}\sqrt{1 - c^2}\, I_1 - \frac{1}{2}\, I_2 \tag{40}$$

where $$I_1 = \int_{x_2}^{1} \frac{\sqrt{\frac{1}{c^2} - x}}{\sqrt{x(x - x_2)(1 - x)(x_3 - x)}}\, dx \tag{41}$$

and $$I_2 = \int_{x_2}^{1} \left[\frac{\left(\frac{1}{c^2} - x\right)\left(1 - x\right)}{x(x - x_2)(x_3 - x)} \right]^{\frac{1}{2}} dx \qquad (42)$$

To evaluate these integrals, we make use of series expansions of the type given in Equations 38 and 39, thus obtaining for I, the series of integrals

$$I_1 = \sqrt{\frac{1 - c^2}{c^2(x_3 - 1)}} \left\{ \sum_{j=0}^{\infty} A_j \int_{x_2}^{1} \frac{(1 - x)^j}{\sqrt{(1 - x)(x - x_2)}} dx \right\}$$

$$= \frac{1}{c} \sqrt{\frac{1 - c^2}{x_3 - 1}} \sum_{j=0}^{\infty} A_j I^{(j)}$$

where the A_j are constants to be given below. The integrals, $I^{(j)}$, are evaluated easily; make the substitution

$$\sin^2\psi = \frac{x - x_2}{1 - x_2}$$

Then $$I^{(j)} = \int_{x_2}^{1} \frac{(1 - x)^j}{\sqrt{(1 - x)(x - x_2)}} dx = 2(1 - x_2)^j \int_0^{\pi/2} \cos^{2j} \psi \, d\psi$$

$$= \frac{(2j)! \, \pi(1 - x_2)^j}{2^{2j} (j!)^2} \qquad (43)$$

Hence
$$I_1 = \frac{\pi}{c}\sqrt{\frac{1 - c^2}{x_3 - 1}} \left\{ \sum_{j=0}^{\infty} A_j \frac{(2j)!(1 - x_2)^j}{2^{2j}(j!)^2} \right\} \qquad (44)$$

Similarly

$$I_2 = \frac{\pi}{c}\sqrt{\frac{1 - c^2}{x_3 - 1}} \left\{ \sum_{j=0}^{\infty} A_j \frac{(2j + 2)! \; (1 - x_2)^{j+1}}{2^{2j+2}\left[(j + 1)!\right]^2} \right\} \tag{45}$$

By carrying out the series expansions for the integrands in Equations 41 and 42 as discussed above, the A_j are found as the following series, which make the expansions for I_1 and I_2 accurate at least to order $(1/K^4)$.

$$\begin{aligned}
A_0 &= 1 \\
A_1 &= \frac{1}{2}\left[1 - \frac{4c^4}{K^2(1 - c^2)} + \ldots\right] \\
A_2 &= \frac{3}{8} + \frac{c^6}{K^2} \frac{3c^2 - 1}{(1 - c^2)^3} + \ldots \\
A_3 &= \frac{5}{16} + \ldots
\end{aligned} \tag{46}$$

The condition for a closed-loop meridian curve is $z(x_2) = 0$, or from Equation 40

$$I_1 = \frac{K}{2\sqrt{1 - c^2}} I_2 \tag{47}$$

To evaluate the conditions required by this equation, the terms $(1 - x_2)^j$ must be expanded in powers of $(1/K)$. We obtain

$$\sum_{j=0}^{\infty} A_j \frac{(2j)!\,(1-x_2)^j}{2^{2j}(j!)^2} = 1 + \frac{1}{K}\sqrt{1-c^2} + \frac{9-13c^2}{4K^2}$$

$$+ \frac{25 - 93c^2 + 127c^4 - 75c^6}{4K^3(1-c^2)^{3/2}} + \ldots$$

$$\sum_{j=0}^{\infty} A_j \frac{(2j+2)!\cdot(1-x_2)^{j+1}}{2^{2j+2}\left[(j+1)!\right]^2} = \frac{2}{K}\sqrt{1-c^2}\left[1 + \frac{3-5c^2}{2K\sqrt{1-c^2}}\right.$$

$$\left. + \frac{15 - 42c^2 + 43c^4}{4K^2(1-c^2)} + \frac{175 - 705c^2 + 1005c^4 - 891c^6}{16K^3(1-c^2)^{3/2}} + \ldots\right] \quad (48)$$

Substituting Equation 48 into 47 and collecting like terms in $(1/K)$, we find

$$\frac{1-3c^2}{2K\sqrt{1-c^2}} + \frac{3 - 10c^2 + 15c^4}{2K^2(1-c^2)} + \frac{75 - 332c^2 + 497c^4 - 591c^6}{16K^3(1-c^2)^{3/2}} + \ldots = 0$$

Solving for c^2 from the leading term

$$c^2 = \frac{1}{3} + \frac{3 - 10c^2 + 15c^4}{3K\sqrt{1-c^2}} + \frac{75 - 332c^2 + 497c^4 - 591c^6}{24K^2(1-c^2)} + \ldots \quad (49)$$

This equation can be solved for c^2 as an expansion in $(1/K)$ by iteration; thus from the first term

$$c^2 = \frac{1}{3} + \ldots$$

Substituting this result into the leading two terms on the right side of Equation 49 yields

$$c^2 = \frac{1}{3} + \left(\frac{2}{3}\right)^{3/2} \frac{1}{K} + \dots$$

Substituting this into the leading three terms on the right of Equation 49

$$c^2 = \frac{1}{3} + \left(\frac{2}{3}\right)^{3/2} \frac{1}{K} + \frac{11}{144} \frac{1}{K^2} + \dots \tag{50}$$

The leading term in Equation 50, $c^2 = 1/3$, is identified as the solution for the circular cylinder, which is the undeformed initial state. The second term, then, represents the first order effect of bending. The inverse of Equation 50 is

$$\frac{1}{K} = \left(\frac{3}{2}\right)^{3/2} \left(c^2 - \frac{1}{3}\right) - \frac{11}{144}\left(\frac{3}{2}\right)^{9/2} \left(c^2 - \frac{1}{3}\right)^2 + \dots$$

We are now in a position to evaluate all the properties of the deformed state by series expansion. The filament length for a half-turn is given by Equation 27. Carrying out the expansion of the integrand yields

$$L_2 = \frac{1}{Kc}\sqrt{\frac{1 - c^2}{x_3 - 1}} \left\{ I^{(0)} - \frac{3c^2 - 1}{2K(1 - c^2)} I^{(1)} + \frac{3}{8K} I^{(2)} + 0\left(\frac{1}{K^4}\right) \right\}$$

Substituting the above expansions for c , x_2 , and x_3 , we find

$$L_2 = \frac{\pi}{K} \left[1 - \frac{1}{2K^2} + \dots \right] \tag{51}$$

With this result we find

$$r_1 = \frac{\ell}{L} = \frac{K\ell_2}{\pi}\left[1 + \frac{1}{2K^2} + \ldots\right] \tag{52}$$

and from Equation 26

$$\varphi_2 = cL_2 = \frac{\pi}{\sqrt{3K}}\left[1 + \left(\frac{2}{3}\right)^{\frac{1}{2}}\frac{1}{K} - \frac{23}{32}\frac{1}{K^2} + \ldots\right] \tag{53}$$

The volume is evaluated in a similar way, beginning with Equation 33. Expanding the integrand as above, we find

$$V = \frac{2\varphi\, r_1^3}{3Kc}\sqrt{\frac{1 - c^2}{x_3 - 1}}\left\{I^{(0)} - \frac{1}{2}\left[\frac{3c^2}{1 - c^2} - 1 + \frac{1}{x_3 - 1}\right] I^{(1)} + \frac{5}{8} I^{(2)} + \ldots\right\}$$

where the error term is of order $(1/K^4)$. Note that the coefficient of $I^{(2)}$ has been evaluated at $c^2 = 1/3$, $x_3 = 3$. Substituting for the $I^{(j)}$ from Equation 43 and carrying out the remaining expansions, we find

$$V = \frac{2\varphi\, r_1^3}{3K^2}\left[1 - \left(\frac{2}{3}\right)^{\frac{1}{2}}\frac{1}{K} - \frac{1}{2K^2} + \ldots\right] \tag{54}$$

Now, multiplying the expansions in Equations 53 and 54 produces

$$V_2 = \frac{2\pi^2\, r_1^3}{3\sqrt{3}\, K^3}\left[1 - \frac{181}{96}\frac{1}{K^2} + \ldots\right]$$

However, r_1 is not constant during bending; substituting from Equation 52 yields

$$V_2 = \frac{2\ell_2^3}{3\sqrt{3}\pi}\left[1 - \frac{37}{96}\frac{1}{K^2} + \dots\right] \tag{55}$$

Note that the first term is just the volume of the undeformed cylinder.

The applied bending moment can be found from Equation 35. To first order, $M \propto \varphi$ and $p \approx$ constant. Hence

$$\frac{1}{2} M\varphi = - p \ \Delta V \tag{56}$$

Substituting from Equation 53 and 55, we find the bending-stiffness formula for small deformations in terms of the tube diameter, d, and length, b, of the initially undeformed cylinder

$$\frac{M}{p_0 \ V_0} = \frac{37}{32\sqrt{2}\pi}\left(\frac{\varphi d}{b}\right) \tag{57}$$

Finally the slip condition, $F = F_{lim}$, given by Equation 20 can be evaluated more simply for small deformations. Substituting our expansions for c^2 and x_3, we find

$$\left(\frac{F}{F_{lim}}\right) \underset{K \to \infty}{\sim} \frac{3}{2\sqrt{2}}\frac{1}{f}\sqrt{(1 - x)(x - x_2)} \tag{58}$$

The function $\left[(1 - x)(x - x_2)\right]^{1/2}$ has its maximum at

$$x = \frac{1}{2}(1 + x_2)$$

The value of this maximum is

$$\left[(1 - x)(x - x_2)\right]^{\frac{1}{2}}_{max.} = \frac{1 - x_2}{2} \underset{K \to \infty}{\sim} \frac{2}{K}\sqrt{1 - c^2} \underset{K \to \infty}{\sim} \frac{2\sqrt{2}}{\sqrt{3K}}$$

The incipient-slip condition is $F/F_{lim} = 1$; thus we find from Equation 58 for small f (large K)

$$K_{slip} = \frac{\sqrt{3}}{f} \tag{59}$$

Substituting this result into Equation 53, we find for the bending angle for incipient slip

$$(\varphi_2)_{slip} = \frac{f\pi}{3} \tag{60}$$

and for the bending moment

$$M_{slip} = \frac{37}{72\sqrt{3}\pi^2} f\, p\, \ell_2^3 = \frac{37}{384\sqrt{2}} f\, p\, d^3 \tag{61}$$

All these formulas may be regarded as the leading term in a series expansion in powers of the friction coefficient, f . From this point of view, a value of about $1/2$ is as large as may be allowed for validity of these formulas for incipient slip. The corresponding bending angle is $\varphi_2 = 30°$. It is interesting to note that slip first occurs at the mean radius (for small f), forming an annulus over which the geometric mesh constraint, Equation 6, no longer holds.

SLIP CONDITION FOR A THREE-FIBER FILAMENT-WOUND CYLINDER

The foregoing analysis treated the case of a two-fiber pressure vessel, for which bending deformation was allowed by kinematic shear of the elementary mesh pattern, the stiffness being provided by pressure-volume work. If in addition to these two helically wound fibers, a third family of parallel circles is added, the fiber pattern becomes a structure (so long as starting friction is not exceeded) which will not deform if the fibers are inextensible. The pressure now serves to prevent buckling.

We now resort to membrane theory to calculate the stress resultants, since the shape of the three-fiber cylindrical shell is known a priori. From Flugge (Ref. 5) the solution of the equilibrium equations for a circular cylinder is

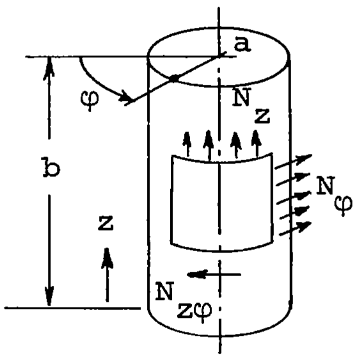

$$N_{\varphi} = pa \tag{62}$$

$$N_{z\varphi} = f_1\ (\varphi) \tag{63}$$

$$N_z = -\left(\frac{z}{a}\right) f_1'\ (\varphi) + f_2\ (\varphi) \tag{64}$$

where the notation is indicated in the sketch. We see that $f_2(\varphi)$ is just N_z at $z = 0$. Hence

$$[N_z]_{z=b} = -\left(\frac{b}{a}\right) f_1'\ (\varphi) + [N_z]_{z=0}$$

By symmetry of the problem, we set $[N_z]_{z=b} = [N_z]_{z=0}$, or

$$f_1'\ (\varphi) = 0$$

Hence $$N_{z\varphi} = f_1 = \text{constant}$$

and $$N_z = f_2\ (\varphi) = [N_z]_{z=0}$$

Note that $N_{z\varphi}$ constant implies torsion. Hence we set

$$N_{z\varphi} = 0$$

Now consider the tension in the fibers. Let n'_C be the number of fibers per unit length, along z , of the parallel-circle fibers, and n'_L and n'_R those of the left- and right-running helically wrapped fibers. For a symmetric pattern, $n'_L = n'_R$. Then from the geometry of the mesh pattern, we have the following local equilibrium conditions. For equilibrium in the z-direction

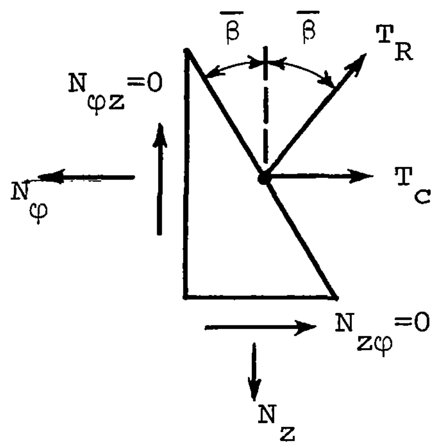

$$2n'_R\ T_R\ \cos\overline{\beta} = N_z\ \tan\overline{\beta} \tag{65}$$

and in the direction normal to T_R

$$n'_C\ T_C\ \cos\overline{\beta} = N_\varphi\ \cos\overline{\beta} - N_z\ \sin\overline{\beta}\ \tan\overline{\beta} \tag{66}$$

Also by symmetry, $T_L = T_R$. Note that $\bar{\beta}$ as used here is the complement of β as used in the preceding two-fiber analysis, because the coordinate system is defined differently.

Now let us require that the tensile stress resultant in the shell vary as cosine φ ; then from overall equilibrium of the cylindrical shell

$$N_\varphi = pa \tag{67}$$

$$N_z = \frac{1}{2} pa + B \cos\varphi \tag{68}$$

where B is a constant to be determined from the applied moment. Then the fiber tension is

$$n_L' T_L = n_R' T_R = \frac{1}{4} pa \sec\bar{\beta} \tan\bar{\beta} + \frac{B}{2} \tan\bar{\beta} \sec\bar{\beta} \cos\varphi \tag{69}$$

$$n_C' T_C = pa \left(1 - \frac{1}{2} \tan^2 \bar{\beta}\right) - B \tan^2 \bar{\beta} \cos\varphi \tag{70}$$

The frictional force on the fibers is determined readily. Since the three-fiber winding pattern is undeformed in the pre-slip loading condition, the fibers have no geodesic curvature. As a result, the frictional forces are parallel to the fibers. They are determined by considering equilibrium parallel to the fibers:

$$F = \frac{dT}{d\ell}$$

or, with $d\ell = a \csc \bar{\beta}\, d\varphi$, we have

$$F_C = \frac{1}{a} \frac{dT_C}{d\varphi} , \qquad F_{L,R} = \frac{1}{a} \sin\bar{\beta} \frac{d\, T_{LR}}{d\varphi} \tag{71}$$

Hence from Equations 69 and 70

$$F_C = \frac{B}{n_C' a} \tan^2 \bar{\beta} \sin\varphi \tag{72}$$

$$F_L = F_R = -\frac{B}{2n_L' a} \tan^2 \bar{\beta} \sin\varphi \tag{73}$$

The frictional starting force should be proportional to the normal force between overlying fibers. An element of area, $a(dz)(d\varphi)$, supports the pressure load, $pa\ dzd\varphi$, while the fibers support a radial pressure load, $(n_C' T_C/a)$, for the parallel circles and $(n_L' T_L \sin\bar{\beta}/a)$ for each family of helical fibers. (This may be confirmed by summing the formulas (65) and (66) for the tensions, T_C and T_L). The total length of fiber per unit area is just n_C' for the parallel circles and $n_L' \csc\bar{\beta}$ for the helices. Hence the normal force per unit length sustained by each fiber is (T_C/a), $(T_L/a) \sin^2 \bar{\beta}$, and $(T_R/a) \sin^2 \bar{\beta}$. Thus for the starting friction on the outer, right-running layer, we have

$$\begin{aligned} \left[F_R\right]_{lim} &= f(T_R/a) \sin^2 \bar{\beta} \\ &= \frac{1}{2}\left(\frac{f}{n_L' a}\right)\left[\frac{pa}{2} + B \cos\varphi\right] \sin\bar{\beta} \tan^2 \bar{\beta} \end{aligned} \tag{74}$$

where we have assumed the helical wrap to be outermost. As a special case, put $\tan^2 \bar{\beta} = 2$ (or $c^2 = 1/3$). Then $T_C = 0$ for $B = 0$, and Equation 74 reduces to the two-fiber result given by Equation 18. For the three-fiber mesh, Equations 73 and 74 yield

$$F_R \Big/ F_{R_{lim}} = -\frac{B \csc\bar{\beta} \sin\varphi}{f(\frac{1}{2} pa + B \cos\varphi)} \tag{75}$$

For small f , B is small also, and so for $F_R = (F_R)_{lim}$

$$B_{slip} = \frac{1}{2} f \, pa \sin\overline{\beta} \qquad (76)$$

for the starting-slip condition on the outer helical fiber layer.

The bending moment is now calculated from the axial stress resultant given by Equation 68:

$$M = a^2 \int_0^{2\pi} N_z \cos\varphi \, d\varphi = a^2 \int_0^{2\pi} (\frac{1}{2} pa + B \cos\varphi) \cos\varphi \, d\varphi$$

Carrying out the integration and substituting for B from Equation 76, we find the limiting bending moment without fiber slippage:

$$M_{slip} = \frac{\pi}{2} f \, pa^3 \sin\overline{\beta} \qquad (77)$$

Again evaluating the two-fiber limit by setting $\sin^2\overline{\beta} = 2/3$, we find that Equation 77 yields a value about twice that given by Equation 61. The discrepancy is accounted for by recalling that Equation 77 was derived for a non-deforming mesh, as required for a three-fiber pattern, whereas Equation 61 is based on a deforming two-fiber mesh, including volume change. Note from Equations 50 and 53 that c increases with bending, corresponding to $\overline{\beta}$ decreasing, thus reducing the value of Equation 77 in the two-fiber limit. With the third family of parallel-circle fibers, the winding angle of the helical fibers will have a higher advance ratio, since the helices support the full pressure load on the end caps, but not along the length of the cylinder.

THE POSTSLIP PHASE

The results of the small deformation analysis for two-fiber tubes showed that fiber slippage occurs over an annular region about the mid-radius of the deformed tube. This annular slip region is, of course, bounded by two regions in which slip has not yet occurred, one at the outer radius and one at the inner radius. Consequently, the equations already developed for the preslip phase hold locally in the two no-slip regions for the postslip phase. However, the equilibrium equations for the slip region cannot be reduced to the same degree of simplicity as for the no-slip region. In particular, the solution for the shape of the meridian curve involves simultaneous integration of first-order differential equations for z, p, and T. These equations are derived readily from Equation 3 and either Equation 19 for the filament-wound tube or Equation 23 for the linked-fiber tube. These integral curves must satisfy appropriate matching conditions at the juncture with the no-slip region.

The resulting equations for the filament-wound tube are listed below:

$$\frac{dZ}{dR} = - \cot\alpha \tag{78}$$

$$\frac{d}{dR}(\sin\beta) = \frac{f\ K\ R\ \cos^2\beta}{\left(\frac{T}{T_1}\right)\sin\alpha} - \frac{\sin\beta}{R} \tag{79}$$

$$\frac{d}{dR}\left(\frac{T}{T_1}\right) = \frac{f\ K\ R\ \sin\beta}{\sin\alpha} \tag{80}$$

The fourth unknown, α, is obtained by direct integration of Equation 4, which holds over both preslip and postslip regions. The result is

$$\cos\alpha = \frac{\sqrt{1 - c^2} - \frac{1}{2} K\ (1 - R^2)}{\left(\frac{T}{T_1}\right)\cos\beta} \tag{81}$$

A set of equations very similar to Equations 78 through 81 holds for the linked-fiber tube.

In addition to the equations given above, integrals for fiber length, bending angle, and tube volume are formulated as for the preslip bending state. However, the energy method used there to determine the bending moment no longer applies because energy is lost in fiber slippage. Instead, a direct integration of the moment contributions of fiber tension and pressure can be used:

$$\frac{d}{dR}\left(\frac{M}{pr_1^{\,3}}\right) = 2(1 - R)\left[\frac{1}{K}\left(\frac{T}{T_1}\right)\frac{\sin\beta\,\tan\beta}{R\,\sin\alpha} - Z\right] \qquad (82)$$

To assess the qualitative effects of fiber slippage, consider the case of frictionless fibers. In the limit, $f \rightarrow 0$, Equation 80 yields $T = T_1$, and Equation 79 yields $R \sin\beta$ = constant. These are just the conditions for isotensoid fiber shells. In Reference 1 it was shown that the integrals for the meridian curve, $z(R)$, fiber length, L , angle, φ , and volume, V , could be evaluated for the isotensoid shell in terms of elliptic integrals. For a torus, each of these elliptic-integral expressions can be expanded in a series of powers of the modulus, k , given by

$$k^2 = \frac{1 - x_2}{1 - x_3}$$

where x_2 and x_3 are roots of $\sin\alpha = 0$, given by an equation similar to Equation 12. The development of these series expansions is quite similar to that carried out in a previous section. The pertinent results are as follows:

$$x_2 = 1 - k^2 - \frac{1}{8}k^6 - \frac{1}{16}k^8 - \frac{57}{1024}k^{10} + \ldots$$

$$x_3 = -\frac{1}{8}k^4 - \frac{1}{16}k^6 - \frac{57}{1024}k^8 + \ldots$$

$$c = \frac{1}{\sqrt{3}} \left\{ 1 - \frac{1}{4} k^2 - \frac{23}{128} k^4 + \ldots \right\}$$

$$K = 4 \sqrt{\frac{2}{3}} \left\{ \frac{1}{k^2} - \frac{31}{256} k^2 + \ldots \right\}$$

$$\varphi_2 = \frac{\pi}{4\sqrt{2}} \left\{ k^2 + \frac{1}{2} k^4 + \frac{101}{256} k^6 + \ldots \right\}$$

$$V_2 = \frac{\pi^2 r_1^3}{64\sqrt{2}} \left\{ k^6 + \frac{3}{4} k^8 + \frac{215}{256} k^{10} + \ldots \right\}$$

$$L_2 = \frac{\pi}{4} \sqrt{\frac{3}{2}} \left\{ k^2 + \frac{1}{4} k^4 + \frac{51}{256} k^6 + \ldots \right\}$$

The constant, r_1, is not invariant with deformation of the tube. Eliminating it in favor of the invariant, $\ell_2 = L_2 r_1$, we have

$$\frac{V_2}{\ell_2^3} = \frac{2}{3\sqrt{3\pi}} \left\{ 1 + \frac{7}{128} k^4 + \ldots \right\}$$

or in terms of the angle, φ_2

$$\frac{V}{V_0} = 1 + \frac{7}{4\pi^2} \varphi_2^2 + \ldots$$

where V_0 is the volume of the undeformed tube. Now from Equation 35

$$M = - p V_0 \frac{d}{d\varphi_2} \left(\frac{V}{V_0} \right)$$

which yields $$\left(\frac{M}{p_0 V_0}\right) = -\frac{7}{2\pi^2}\varphi_2 + \ldots$$

It is interesting, and exasperating, that terms to order k^{10} in the series for x_2 were necessary to retain only the leading term in the series for the bending moment. For a tube of diameter, d, length b,

$$d = \frac{2\sqrt{2}}{\pi} b_2 = \frac{2\sqrt{2}}{\pi} b \frac{\varphi_2}{\varphi}$$

Thus $$\frac{V}{V_0} = 1 + \frac{7}{32}\left(\frac{\varphi d}{b}\right)^2 + \ldots \tag{83}$$

$$\frac{M}{p V_0} = -\frac{7}{4\sqrt{2}\pi}\left(\frac{\varphi d}{b}\right) + \ldots \tag{84}$$

The negative sign in Equation 84 corresponds to a restraining moment, implying that the frictionless fiber tube is unstable. This fact is also clear from Equation 83 which states that the volume of the tube increases quadratically with bending moment. It is now evident that the two-fiber tube is stabilized only by frictional effects.

Figure 5 shows a plot of Equation 83, together with computed points for a three-fiber frictionless tube having one meridian-wrapped family of fibers ($\beta = 0$) and two symmetric families of fibers ($\beta = \pm 45°$). The density of the meridian-wrapped fibers is $\sqrt{2}$ times that of each of the skewed fibers, to satisfy equilibrium with the pressure on the endcaps. The calculations for the three-fiber tube were carried out in the manner described in Reference 6. From the figure it would seem that the third fiber has no significant effect on the stability of the frictionless tube, at least for the fiber angle chosen. The stabilizing effect of the third fiber that was observed experimentally in Reference 3 is associated with a "pinch effect" in which the bent tube departs from toroidal symmetry. The present analysis, however, does not account for this mode of deformation.

From these results, we conclude that the stable bending conditions derived for small deformations in a previous section come about solely due to friction, and when the frictional limits are exceeded, significant reduction of the bending moment can occur.

NUMERICAL RESULTS FOR THE TWO-FIBER TUBE

In addition to the small-deformation analysis carried out previously, numerical results have been obtained for large deformations by solving the complete equations developed in an earlier section by finite differences. The numerical integration procedure used was the fourth order Runge-Kutta scheme, and the calculations were carried out using an IBM 7094 digital computer. The numerical results were found to be quite sensitive to step size, as determined by comparison with the analytical results for large K and c near $1/\sqrt{3}$. Satisfactory accuracy was obtained by use of 100 steps over the range, $0 \leq \psi \leq \frac{\pi}{2}$, where ψ is defined by Equation 29 for the preslip condition. With this choice the meridian curve, $Z(R)$, is accurate to six significant figures. This degree of accuracy on Z resulted in only 3 or 4 figure accuracy on the value of K required for a closed-loop torus.

Torus solutions were found as follows. Meridian curves were generated by integrating from $\alpha = 0$ $(R = 1)$ to $\alpha = \pi$ $(R = R_2)$ for various values of K, with c fixed, until two values of K are determined for which Z_2 has opposite sign. This interval of K is repeatedly halved until Z_2 is reduced in magnitude to the desired value (10^{-7}). Figure 6 shows typical variations of Z_2 with K for the no-slip condition. The no-slip curve has one zero, yielding torus conditions. The shape of the curve is such that iteration by linear interpolation is exceedingly slow after bracketing the root, and does not work at all before the root is bracketed. On the other hand, the interval-halving technique is quite effective. Note the sensitivity of K to slight changes of Z_2 indicated in the figure.

The results of most interest are the moment-deformation characteristics of the tube. The two solid curves in Figure 7 show bending moment versus bending angle for the no-slip condition as obtained by the numerical integration procedure described above. The dashed line denoted "linear theory" results from Equation 57. The curve labelled "adiabatic" represents the situation in which the gas in the tube is compressed without heat or mass transfer from the tube; the curve labelled "isobaric" represents the situation in which the tube is connected to a large reservoir so that the pressure remains constant during bending. The isothermal process would produce a curve lying between the isobaric and adiabatic curves. The bending moment is observed to rise almost linearly up to a value of 0.8 for the reduced bending angle, $\varphi\, d/b$, followed by a significantly reduced bending stiffness. The knee in the curve is especially evident for the constant-pressure case. A further break in the curve with reduced stiffness would be expected when fiber slippage occurs. The linear variation holds over a remarkably large range of bending, as can be seen by taking an example. For a tube with a length-to-diameter ratio of four, the knee of the curve corresponds to a bending angle of 3.2 radians. In other words, the tube can be bent into a U-shape with a linear bending moment graph.

From Equation 8 as well as Equation 80 it is seen that the maximum value of fiber tension over the tube occurs at maximum radius. Figure 8 shows the variation of this maximum fiber tension with bending angle for no fiber slippage. With constant pressure, the tension is seen to peak at a value about 30 percent greater than the tension in the undeformed tube, with the peak occurring at the approximate knee of the bending moment curve of Figure 7. In contrast, the maximum fiber tension in the tube continues to rise rapidly with bending angle for the adiabatic case, owing to the strongly increasing pressure in the tube.

The results discussed above are restricted to a fiber mesh without slippage. Conditions for incipient slippage of the filament-wound tube are given by Equation 20, which has been evaluated using the results of the numerical integration. These conditions are shown in Figure 9. Clearly a friction coefficient of unity is sufficiently large to prevent slippage over the full range of bending angle considered here. For the linked-fiber tube, the incipient-slip conditions are determined by Equation 25. For small bending deformation, this equation can be expressed as

$$f = \sqrt{6}\,\frac{\varphi_2}{m}$$

where m is the number of fibers crossing a meridian curve of the tube. Comparing with Equation 60, we see that the linked-fiber net is less subject to slippage than the filament-wound shell, if $m > \sqrt{6}\,\frac{\pi}{3}$. This number of fibers will be greatly exceeded in technical applications.

REFERENCES

1. Schuerch, H. U., and Burggraf, O.R.: Analytical Design for Optimum Filamentary Pressure Vessels, AIAA J. Vol. 2, No. 5, pp 809-820, May 1964.

2. Prager, Wm., and Hodge, P.G.: Theory of Perfectly Plastic Solids, Wiley, 1951.

3. Kyser, A.C., and Schuerch, H.U.: Pressurized Structures of High Mobility, Astro Research Corporation ARC-R-221, 1966.

4. Milne-Thomson, L.: Jacobian Elliptic Function Tables, Dover, 1950.

5. Flugge, W.: Stresses in Shells, Springer, 1960.

6. Schuerch, H.U., Burggraf, O.R., and Kyser, A.C.: A Theory and Applications of Filamentary Structures, NASA TN D-1692, 1962.

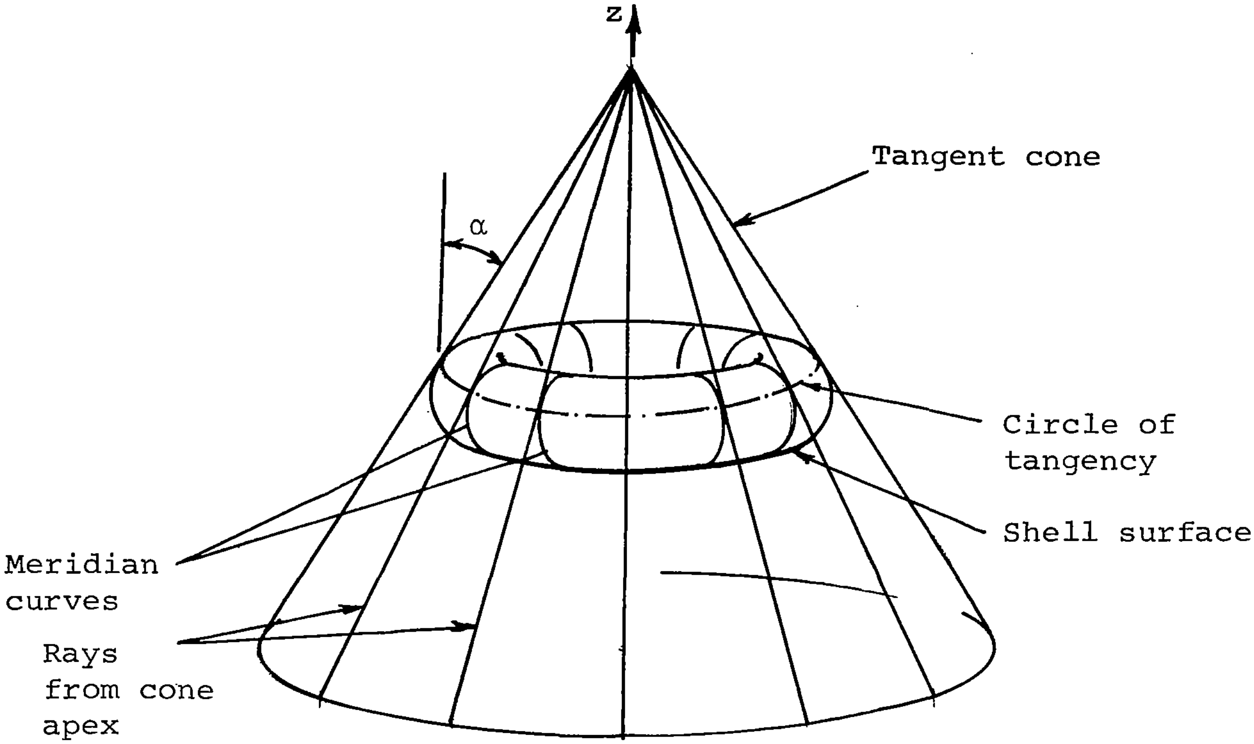

Figure 1. Layout of Deformed Fiber Shell (Extended into a Closed Torus) and Tangent Cone

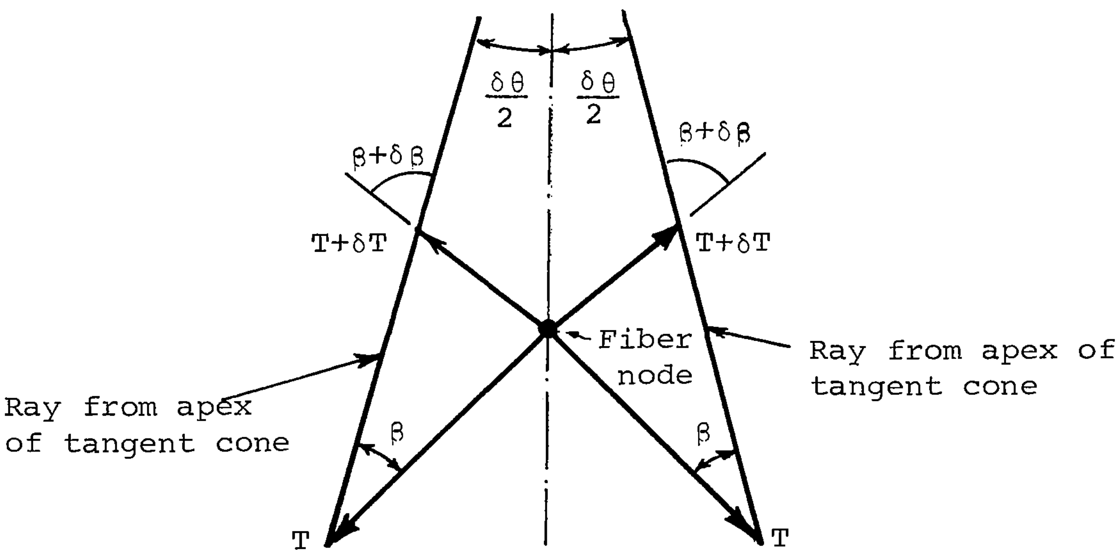

Figure 2. Diagram of Equilibrium of Forces Acting on Fiber Node in Plane Tangent to Surface

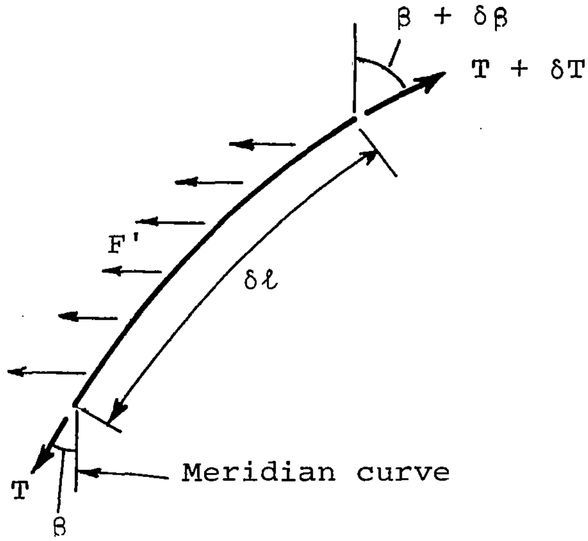

Figure 3. Forces Acting in Tangent Plane on Wound Fiber

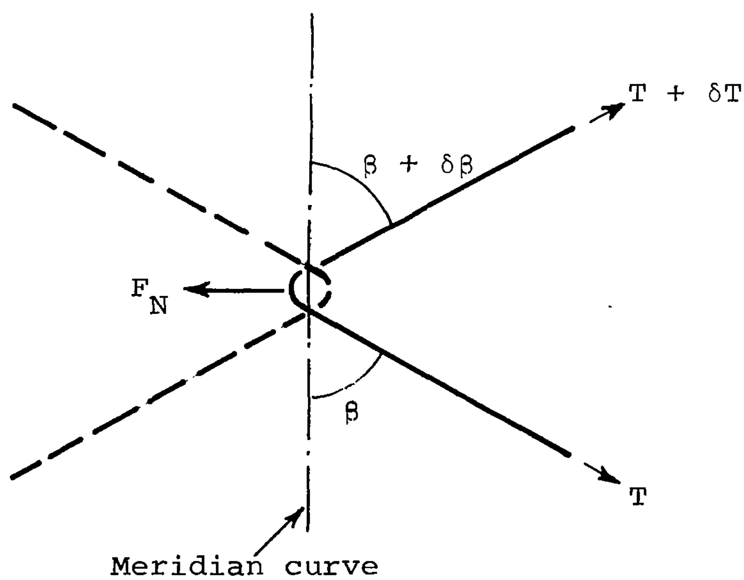

Figure 4. Forces Acting in Tangent Plane on Linked Fiber

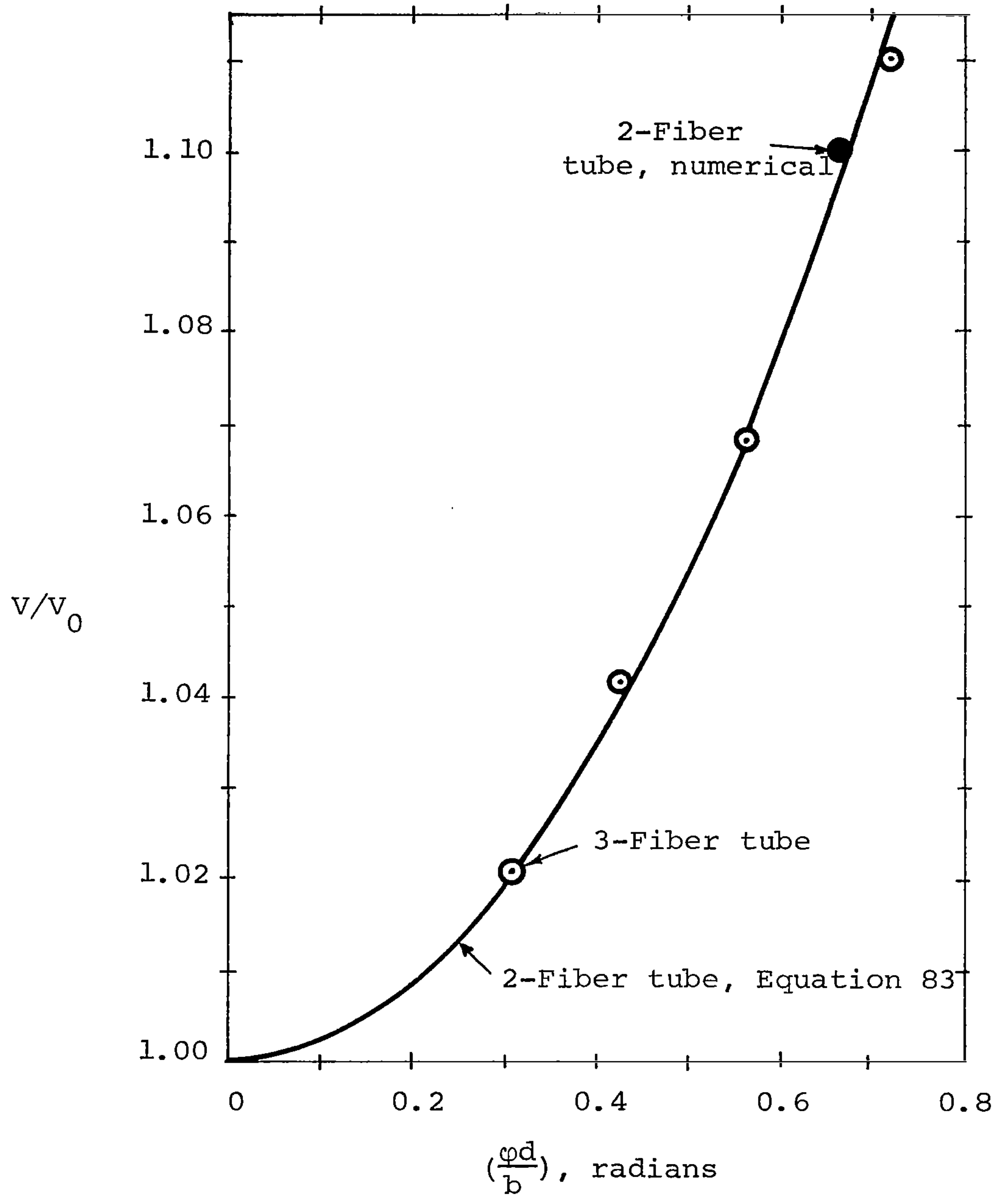

Figure 5. **Volume** Change of Frictionless Fiber Tubes as a Function of Bending Angle

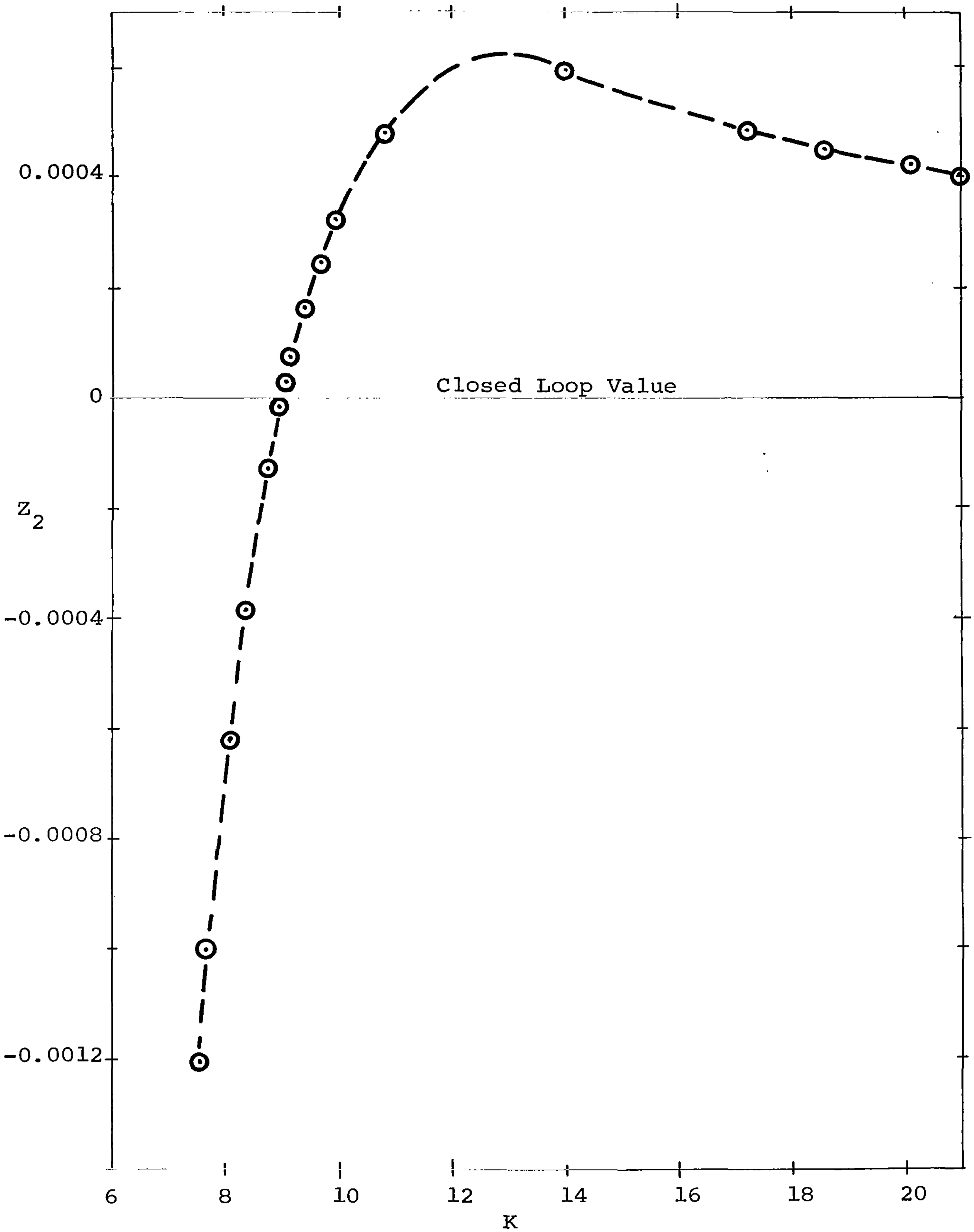

Figure 6. Numerical Results for Z_2 versus K, Illustrating the Method of Generating Torus Conditions

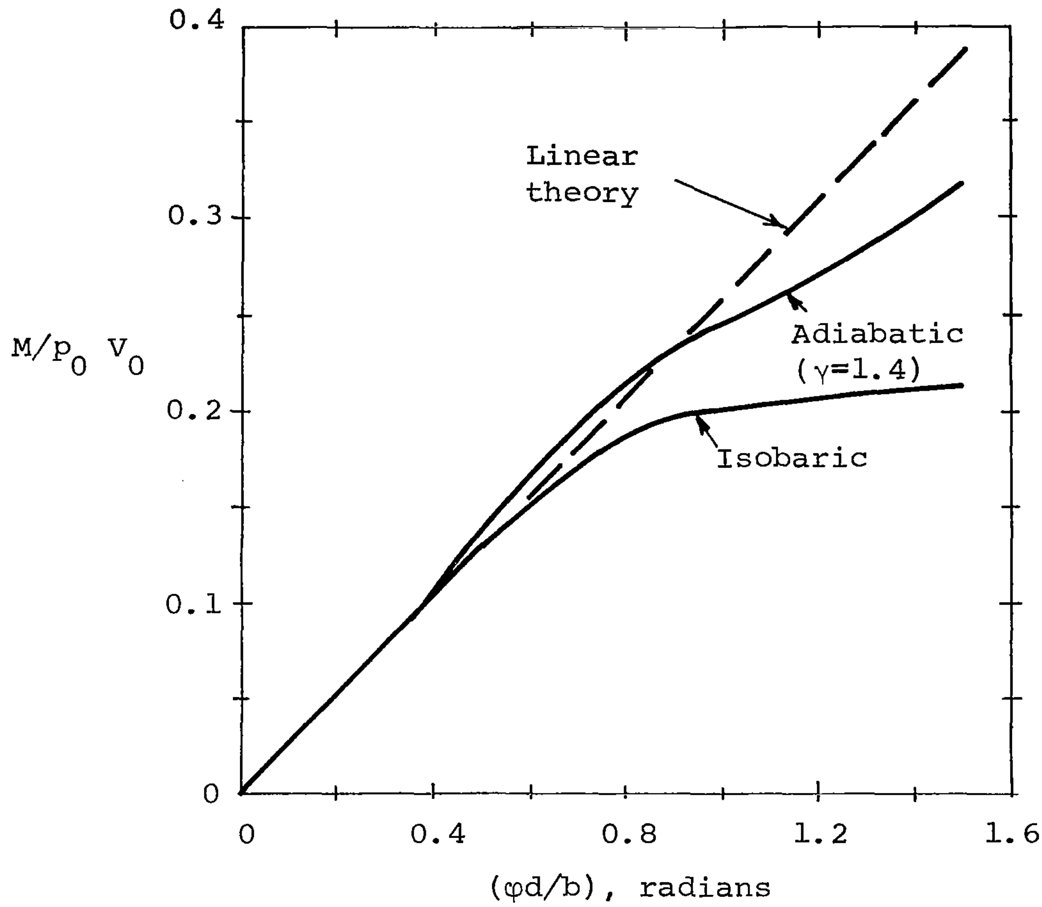

Figure 7. Moment-Deformation Characteristics of Two-Fiber Shell in Preslip Phase of Bending

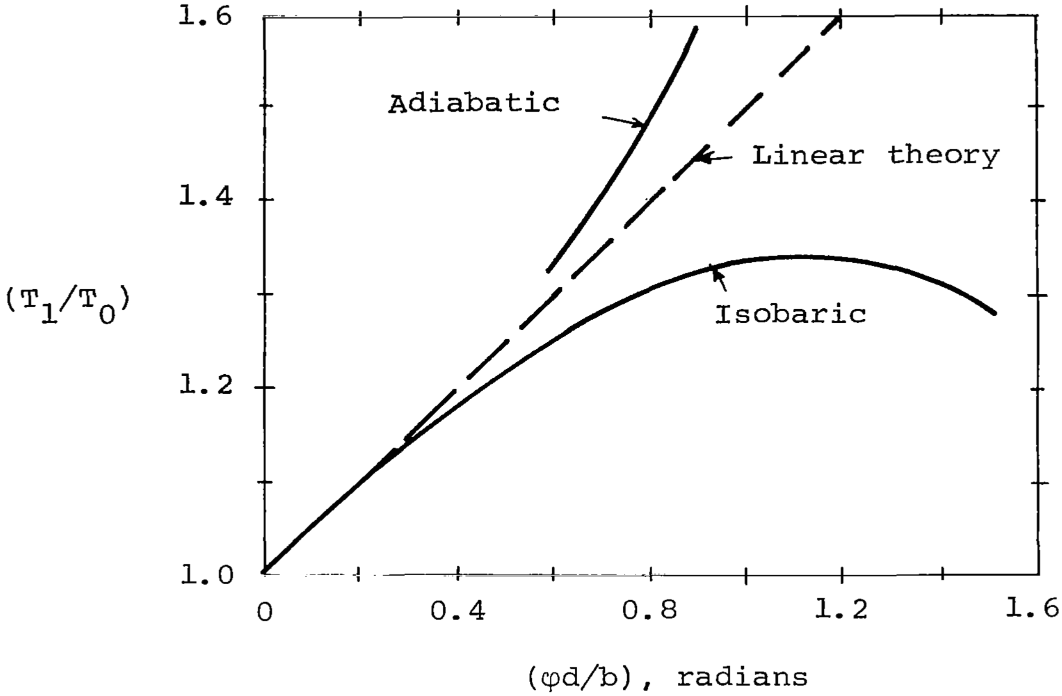

Figure 8. Maximum Fiber Tension versus Bending Angle for Two-Fiber Shell in Preslip Range of Bending

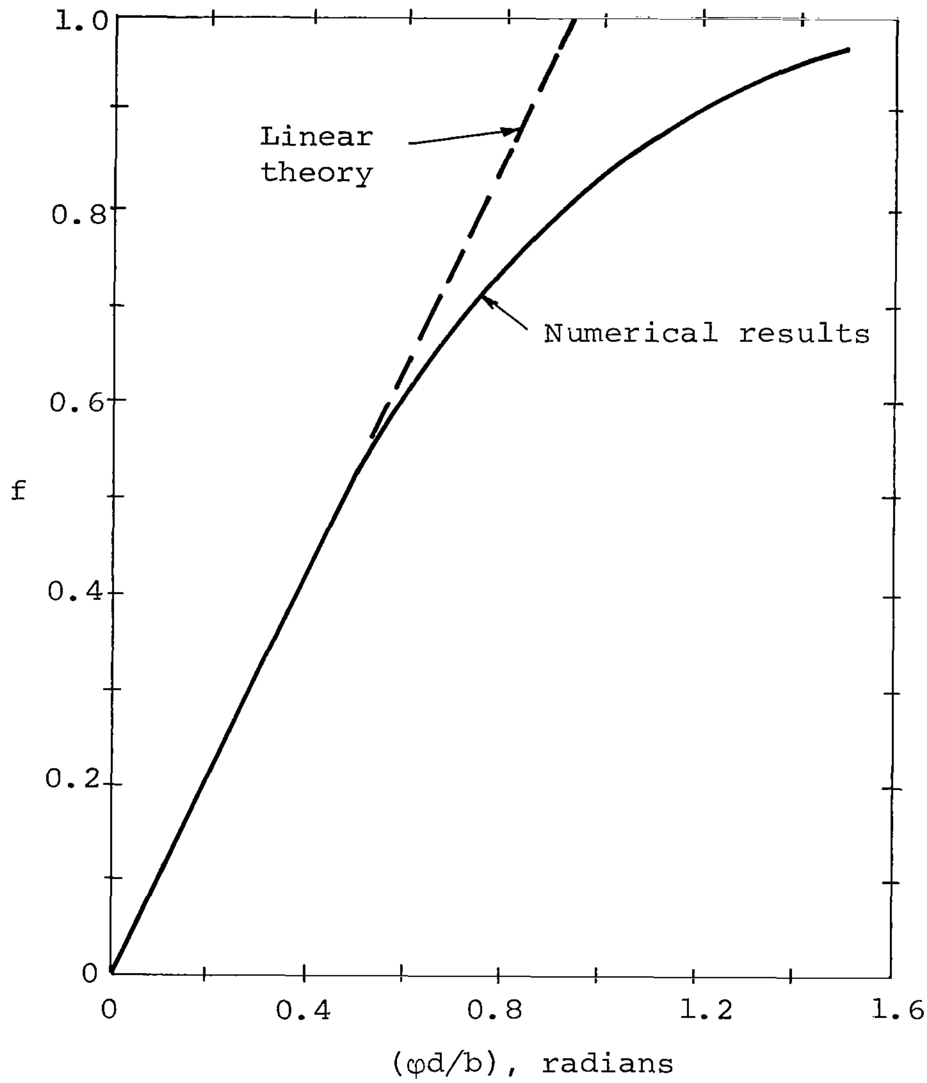

Figure 9. Friction Coefficient for Incipient Fiber Slippage on Filament-Wound Two-Fiber Tube

NASA-Langley, 1969 —— 5 CR-1507